Available online at www.sciencedirect.com
SCIENCE DIRECT®
Journal of Sound and Vibration 263 (2003) 725–742
JOURNAL OF SOUND AND VIBRATION
www.elsevier.com/locate/jsvi

Coupled lateral and torsional vibration characteristics of a speed increasing geared rotor-bearing system

An Sung Lee[a,*], Jin Woong Ha[b], Dong-Hoon Choi[c]

[a] *Rotor Dynamics Group, Korea Institute of Machinery and Materials, Yoosung P.O. Box, 101, Daejeon 305-600, South Korea*
[b] *R&D Department, Century Corporation, Asansi, Chungnam 336-842, South Korea*
[c] *School of Mechanical Engineering, University of Hanyang, Seoul 133-791, South Korea*

Received 14 December 2001; accepted 8 July 2002

Abstract

The goal of this study was to examine the coupled vibration characteristics of a turbo-chiller rotor-bearing system having a bull-pinion speed increasing gear, using a coupled lateral and torsional vibration finite element model of a gear pair, and to provide the mechanism of the characteristic changes. The investigations were systematically carried out by comparing the uncoupled and coupled natural frequencies and their mode shapes with varying gear mesh stiffness, taking into account rotating speeds, and by comparing the strain energies of the lateral and torsional vibration modes. The results show that some modes may yield coupled lateral and torsional mode characteristics when the gear mesh stiffness increases over a certain value and, in addition, that their associated dominant modes may be different from their initial modes, i.e., a given dominant mode may change from an initial torsional one to a lateral one or vice versa.

1. Introduction

It is known that for a general rotor system with a shaft diameter-to-length ratio, D/L, >0.01, the coupled effect of the lateral and torsional vibrations may be neglected [1]. However, for a gear box or geared rotor-bearing system, a coupled phenomenon of the lateral and torsional vibrations may well arise, as the result of gear meshing effects [2]. In particular, for a turbomachine, operating at high speed by means of a speed increasing gear system, the coupled lateral and torsional vibration characteristics may be considerably different from those obtained by uncoupled independent analyses. To achieve a highly reliable design that includes low vibration

*Corresponding author. Tel.: +82-42-868-7356; fax: +82-42-868-7440.
E-mail address: aslee@kimm.re.kr (A.S. Lee).

0022-460X/03/$ - see front matter
PII: S0022-460X(02)01103-3

and noise characteristics for such a high performance machine, an investigation of the coupled lateral and torsional vibration phenomenon which takes the gear meshing effect into consideration would be desirable.

Lund [3] proposed an impedance matching scheme to solve the coupled torsional and lateral vibration in a geared rotor system, utilizing the equations formulated independently by the Holzer method for torsion and the Myklestad–Prohl method for lateral vibration. Iida et al. [4] investigated the coupled torsional–flexural vibration of a flexible shaft driven by a simple spur gear system. They applied a much simple lumped torsional and flexural model, not considering lateral rotary degrees of freedom and treating the driving shaft as laterally rigid. Iwatsubo et al. [5] analyzed the coupled lateral and torsional vibration of a spur-geared rotor system, utilizing the transfer matrix method. In their analysis, the meshing gear teeth were modelled by a simple spring and the gyroscopic moments of gears were not considered. Neriya et al. [6] investigated the dynamic load on gear teeth due to coupling between the flexural and torsional vibrations in a simple geared shaft system. In this study, they applied a coupled vibration model of a gear pair, which took only the translational and torsional degrees of freedom into account. Kahraman et al. [7] carried out an FE dynamic analysis of geared rotor systems, using a coupled vibration model of a gear pair obtained by considering the translational, rotary and torsional degrees of freedom but not the gyroscopic effect, and examined the effect of bearing flexibility on the dynamics of the system. Rao et al. [8] proposed a general FE model of a geared rotor system, which considered the gyroscopic effect, and performed coupled lateral and torsional free vibration analyses of a gear box and a turbo-alternator rotor-bearing system connected by a speed reduction gear. They investigated the effects of gear mesh stiffness on changes in natural frequencies and mode shapes. Lee et al. [9], using a general coupled lateral and torsional vibration FE model of a gear pair, performed a free vibration analysis of a turbo-chiller rotor-bearing system, which contained a speed increasing gear, and investigated the effects of coupled vibrations within its operating speed range. The above investigations treated, in part, some of the characteristic changes of free vibrations which resulted from coupled lateral and torsional vibrations. However, in order to clearly understand the mechanisms behind such characteristic changes, more systematic approaches and detail analyses need to be carried out.

In this study, a general coupled lateral and torsional vibration FE model of a gear pair was used to more precisely examine the coupled vibration characteristics of an 800 refrigeration ton turbo-chiller rotor-bearing system containing a bull-pinion speed increasing gear and to provide the mechanisms of the vibration characteristic changes. The investigations were systematically carried out by comparing the uncoupled and coupled natural frequencies and their mode shapes on varying gear mesh stiffness as well as by comparing the strain energies associated with the lateral and torsional vibration modes.

2. Coupled FE model of gear pair

A displacement vector of a gear pair can be defined from the pressure line co-ordinate system [6,7], as shown in Fig. 1, by

$$\{q^{G'}\} = \left\lfloor u_1^{G'} \;\; v_1^{G'} \;\; \theta_{X1}^{G'} \;\; \theta_{Y1}^{G'} \;\; u_2^{G'} \;\; v_2^{G'} \;\; \theta_{X2}^{G'} \;\; \theta_{Y2}^{G'} \;\; \theta_{Z1}^{G'} \;\; \theta_{Z2}^{G'} \right\rfloor^{\mathrm{T}}, \tag{1}$$

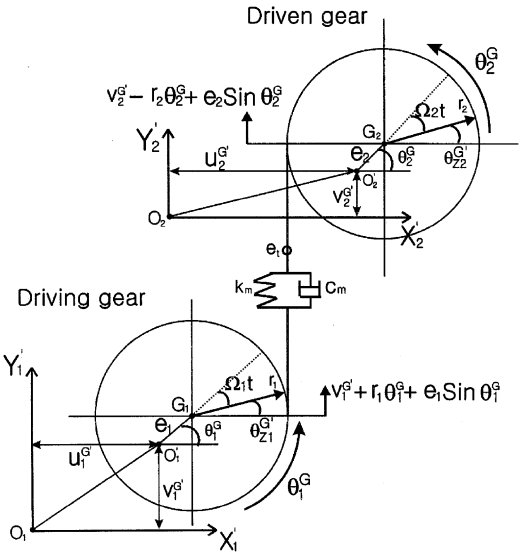

Fig. 1. Co-ordinate systems of a gear pair at the pressure line.

where u, v, θ_X and θ_Y are the lateral degrees of freedom and θ_Z the torsional degree of freedom. Subscripts 1 and 2 indicate the driving and driven gears and superscript G denotes the gear itself. O_1 and O_2 are centers of the gears when they are stationary, O_1' and O_2' centers of the gears when they are rotating, and G_1 and G_2 geometrical centers of the gears. From the equilibria of the force, bending moment and torque for each gear, the equations of motion of a gear pair can be expressed by the following equations:

$$M_1^G \ddot{u}_1^{G'} = U_1 \Omega_1^2 \cos \Omega_1 t, \tag{2}$$

$$\begin{aligned} M_1^G \ddot{v}_1^{G'} + k_m[v_1^{G'} + r_1\theta_1^G - v_2^{G'} + r_2\theta_2^G] + c_m[\dot{v}_1^{G'} + r_1\dot{\theta}_1^G - \dot{v}_2^{G'} + r_2\dot{\theta}_2^G] \\ = U_1\Omega_1^2 \sin \Omega_1 t + k_m[e_2 \sin\theta_2^G - e_1 \sin\theta_1^G + e_t \sin(N_1\Omega_1 t)] \\ + c_m[e_2\Omega_2 \cos\theta_2^G - e_1\Omega_1 \cos\theta_1^G + e_t N_1 \Omega_1 \cos(N_1\Omega_1 t)], \end{aligned} \tag{3}$$

$$M_2^G \ddot{u}_2^{G'} = U_2 \Omega_2^2 \cos \Omega_2 t, \tag{4}$$

$$\begin{aligned} M_2^G \ddot{v}_2^{G'} + k_m[-v_1^{G'} - r_1\theta_1^G + v_2^{G'} - r_2\theta_2^G] + c_m[-\dot{v}_1^{G'} - r_1\dot{\theta}_1^G + \dot{v}_2^{G'} - r_2\dot{\theta}_2^G] \\ = U_2\Omega_2^2 \sin \Omega_2 t - k_m[e_2 \sin\theta_2^G - e_1 \sin\theta_1^G + e_t \sin(N_1\Omega_1 t)] \\ - c_m[e_2\Omega_2 \cos\theta_2^G - e_1\Omega_1 \cos\theta_1^G + e_t N_1 \Omega_1 \cos(N_1\Omega_1 t)], \end{aligned} \tag{5}$$

$$I_{t1}^G \ddot{\theta}_{X1}^{G'} + I_{p1}^G \Omega_1 \dot{\theta}_{Y1}^{G'} = 0, \tag{6}$$

$$I_{t1}^G \ddot{\theta}_{Y1}^{G'} - I_{p1}^G \Omega_1 \dot{\theta}_{X1}^{G'} = 0 \tag{7}$$

$$I_{p1}^{G}\ddot{\theta}_{1}^{G}+k_m[r_1v_1^{G'}+r_1^2\theta_1^G-r_1v_2^{G'}+r_1r_2\theta_2^G]+c_m[r_1\dot{v}_1^{G'}+r_1^2\dot{\theta}_1^G-r_1\dot{v}_2^{G'}+r_1r_2\dot{\theta}_2^G]$$
$$=\{k_m[-v_1^{G'}-r_1\theta_1^G+v_2^{G'}-r_2\theta_2^G]+c_m[-\dot{v}_1^{G'}-r_1\dot{\theta}_1^G+\dot{v}_2^{G'}-r_2\dot{\theta}_2^G]$$
$$+k_m[e_1\sin\theta_1^G-e_2\sin\theta_2^G-e_t\sin(N_1\Omega_1t)]+c_m[e_1\Omega_1\cos\theta_1^G-e_2\Omega_2\cos\theta_2^G$$
$$-e_tN_1\Omega_1\cos(N_1\Omega_1t)]\}e_1\cos\theta_1^G+\{k_m[e_1\sin\theta_1^G-e_2\sin\theta_2^G-e_t\sin(N_1\Omega_1t)]$$
$$+c_m[e_1\Omega_1\cos\theta_1^G-e_2\Omega_2\cos\theta_2^G-e_tN_1\Omega_1\cos(N_1\Omega_1t)]\}r_1, \tag{8}$$

$$I_{t2}^{G}\ddot{\theta}_{X2}^{G'}+I_{p2}^{G}\Omega_2\dot{\theta}_{Y2}^{G'}=0, \tag{9}$$

$$I_{t2}^{G}\ddot{\theta}_{Y2}^{G'}-I_{p2}^{G}\Omega_2\dot{\theta}_{X2}^{G'}=0, \tag{10}$$

$$I_{p2}^{G}\ddot{\theta}_{2}^{G}+k_m[r_2v_1^{G'}+r_2^2\theta_2^G-r_2v_2^{G'}+r_1r_2\theta_1^G]+c_m[r_2\dot{v}_1^{G'}+r_2^2\dot{\theta}_2^G-r_2\dot{v}_2^{G'}+r_1r_2\dot{\theta}_1^G]$$
$$=\{k_m[-v_1^{G'}-r_1\theta_1^G+v_2^{G'}-r_2\theta_2^G]+c_m[-\dot{v}_1^{G'}-r_1\dot{\theta}_1^G+\dot{v}_2^{G'}-r_2\dot{\theta}_2^G]$$
$$+k_m[e_1\sin\theta_1^G-e_2\sin\theta_2^G-e_t\sin(N_1\Omega_1t)]+c_m[e_1\Omega_1\cos\theta_1^G-e_2\Omega_2\cos\theta_2^G$$
$$-e_tN_1\Omega_1\cos(N_1\Omega_1t)]\}e_2\cos\theta_2^G+\{k_m[e_1\sin\theta_1^G-e_2\sin\theta_2^G-e_t\sin(N_1\Omega_1t)]$$
$$+c_m[e_1\Omega_1\cos\theta_1^G-e_2\Omega_2\cos\theta_2^G-e_tN_1\Omega_1\cos(N_1\Omega_1t)]\}r_2, \tag{11}$$

where M_1 and M_2 represent the masses, I_t and I_p the transverse and polar moments of inertia, k_m and c_m the gear mesh stiffness and damping, r_1 and r_2 the gear base circles, U_1 and U_2 the unbalances, e_1 and e_2 the geometrical eccentricities, Ω_1 and Ω_2 the rotation speeds and θ_1 and θ_2 the rotation angles, respectively. Further, $e_t\sin(N_1\Omega_1t)$ represents the transmission error [10] at a gear meshing point with N_1 representing the driving gear teeth number. By simplifying Eqs. (2)–(11), utilizing the relationships of $\theta_1^G=\theta_{Z1}^{G'}+\Omega_1t$, $\theta_2^G=\theta_{Z2}^{G'}+\Omega_2t$, $r_1\Omega_1+r_2\Omega_2=0$, $\theta_{Z1}^{G'}\ll\Omega_1t$ and $\theta_{Z2}^{G'}\ll\Omega_2t$, and finally, by arranging them in a matrix form, the coupled equation of motion of a gear pair can be expressed by

$$[M^{G'}]\{\ddot{q}^{G'}\}+\{[C^{G'}]+[G^{G'}]\}\{\dot{q}^{G'}\}+[K^{G'}]\{q^{G}\}=\{Q^{G'}\}, \tag{12}$$

where $[M^{G'}]$, $[C^{G'}]$, $[G^{G'}]$, $[K^{G'}]$ and $\{Q^{G'}\}$ are the inertia, damping, gyroscopic and stiffness matrices and the external force vector in the local pressure line co-ordinate system, respectively, and are given in Appendix A by Eqs. (A.1)–(A.5). From Eqs. (A.1)–(A.5) it can be seen that the coupling between the lateral and torsional degrees of freedom is due to the gear mesh stiffness and damping. However, the gear mesh damping was not considered in the present study.

On the other hand, a generalized displacement vector of a gear pair can be defined with respect to the global co-ordinate system, as shown in Fig. 2, by

$$\{q^G\}=\lfloor u_1^G\ \ v_1^G\ \ \theta_{X1}^G\ \ \theta_{Y1}^G\ \ u_2^G\ \ v_2^G\ \ \theta_{X2}^G\ \ \theta_{Y2}^G\ \ \theta_{Z1}^G\ \ \theta_{Z2}^G\rfloor^{\mathrm{T}}. \tag{13}$$

The global coupled equation of motion of a gear pair can then be expressed by Eq. (14) through a co-ordinate transformation:

$$[M^G]\{\ddot{q}^G\}+\{[C^G]+[G^G]\}\{\dot{q}^G\}+[K^G]\{q^G\}=\{Q^G\}, \tag{14}$$

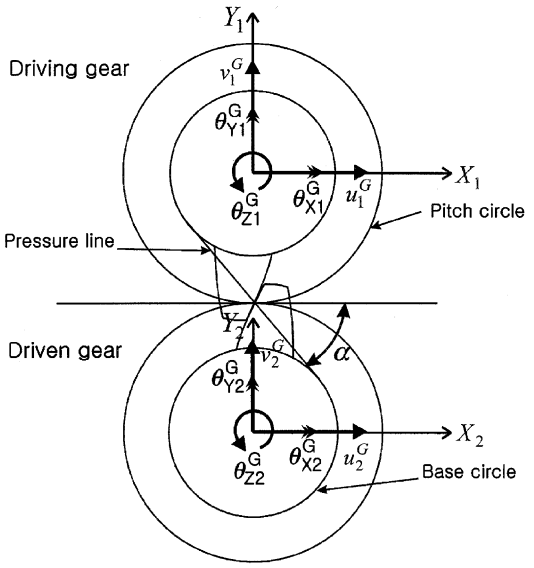

Fig. 2. Global co-ordinate systems of a gear pair.

where the global inertia, damping, gyroscopic and stiffness matrices and the global force vector are obtained by Eqs. (15)–(19) and constitute the coupled vibration FE model of a gear pair:

$$[M^G] = [T][M^{G'}][T]^{\mathrm{T}}, \tag{15}$$

$$[C^G] = [T][C^{G'}][T]^{\mathrm{T}}, \tag{16}$$

$$[G^G] = [T][G^{G'}][T]^{\mathrm{T}}, \tag{17}$$

$$[K^G] = [T][K^{G'}][T]^{\mathrm{T}}, \tag{18}$$

$$\{Q^G\} = [T]\{Q^{G'}\}, \tag{19}$$

where the co-ordinate transformation matrix, $[T]$, is obtained by considering the pressure angle, α, and is given in Appendix A by Eq. (A.8).

Fig. 3 shows the structure of the coupled gear mesh stiffness matrix, $[K^G]$. k_l and k_{lc} represent the pure lateral component and the coupled component between the lateral vibrations and k_t and k_{tc} the pure torsional component and the coupled component between the torsional vibrations, respectively. In addition, k_{tl} represents the coupled lateral and torsional component. In order to construct an entire system equation, an assembly of the derived coupled vibration FE model of a gear pair and the existing lateral and torsional vibration FE models of the shafts, bearings and disks [11] may be readily implemented by placing the matrices of the pure lateral and torsional vibrations diagonally and the matrices of the coupled vibrations off-diagonally (see Fig. 4, which shows the arrangement of an entire assembled stiffness matrix).

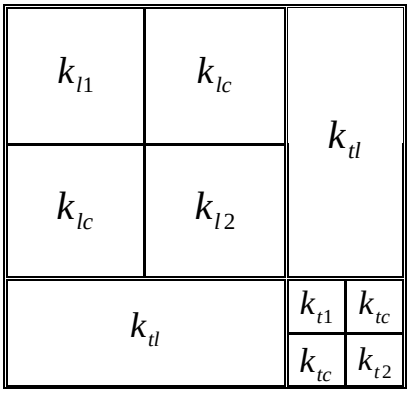

Fig. 3. Structure of a coupled gear mesh stiffness matrix.

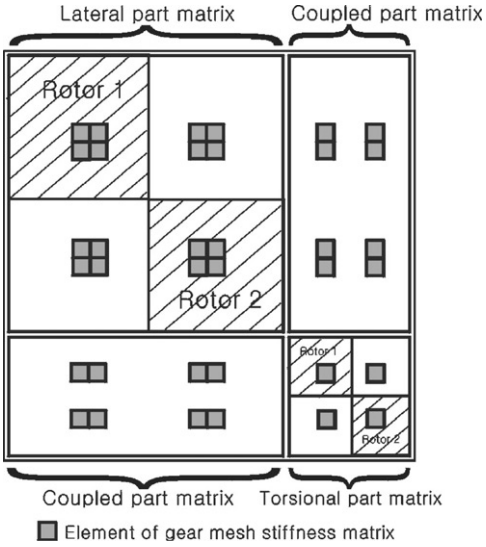

Fig. 4. Structure of an entire assembled stiffness matrix.

3. Results and discussions

By applying the coupled lateral and torsional vibration FE model of a gear pair to an 800 refrigeration ton turbo-chiller rotor-bearing system, uncoupled and coupled free vibration analyses and calculations of the strain energies of the lateral and torsional modes were carried out. In this instance, uncoupled analyses were performed, excluding k_{tl}, k_l and k_{lc} components from $[K^G]$ of Fig. 3. The exclusion of the k_l and k_{lc} components assumes the complete isolation of any gear meshing effect from the lateral vibrations. The coupled analyses were performed so as to include all the components of $[K^G]$. Fig. 5 shows a schematic of the turbo-chiller in which the motor driver, having a rated speed of 3420 r.p.m., drives the compressor impeller to a rated speed

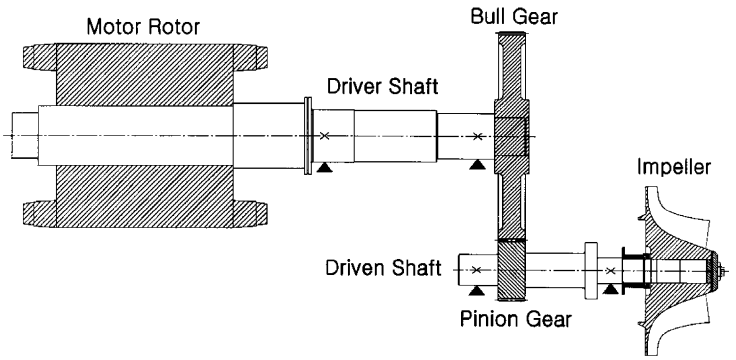

Fig. 5. Schematic of a 800 RT turbo-chiller rotor-bearing system.

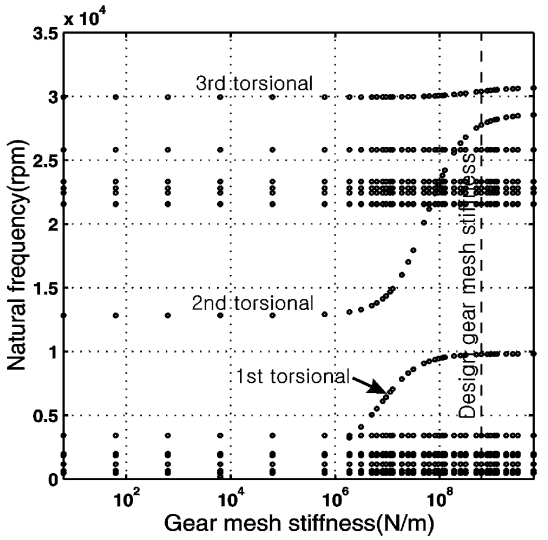

Fig. 6. Natural frequencies versus gear mesh stiffness for an uncoupled analysis at 0 r.p.m.

of 11 845 r.p.m. through a bull-pinion speed increasing gear. In addition, the design gear mesh stiffness, $k_m = 6.31 \times 10^8$ N/m, of the speed increasing gear were calculated from the relationships between the applied gear loads and the resulting bending and compressional displacements [12].

3.1. Natural frequency and mode versus gear mesh stiffness at a motor speed of 0 r.p.m.

3.1.1. Uncoupled analysis

Fig. 6 shows the uncoupled lateral and torsional natural frequencies versus the gear mesh stiffness, k_m. As k_m increases, three natural frequencies change while others remain constant. The former and latter represent the torsional and lateral natural frequencies, respectively. The first torsional natural frequency begins to appear at around $k_m = 1 \times 10^4$ N/m, increases greatly between $k_m = 1 \times 10^6$ and 1×10^8 N/m and thereafter reaches a constant value. The second

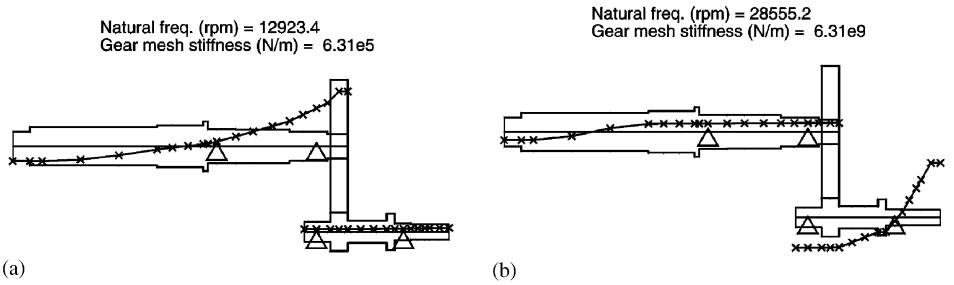

Fig. 7. Second torsional modes for the torsional analysis only at different gear mesh stiffnesses. (a) $k_m = 6.31 \times 10^5$ N/m; (b) $k_m = 6.31 \times 10^9$ N/m.

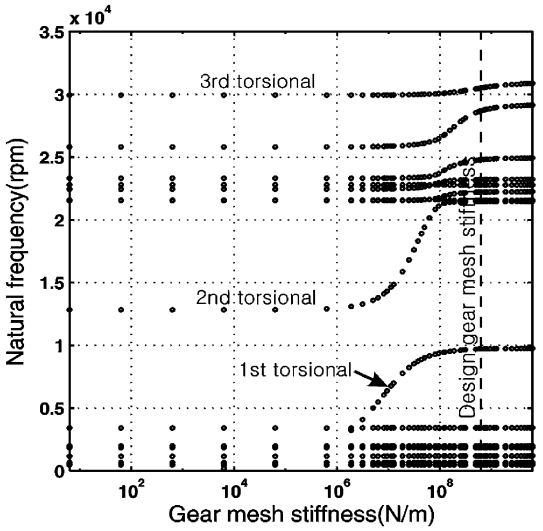

Fig. 8. Natural frequencies versus gear mesh stiffness for a coupled analysis at 0 r.p.m.

torsional natural frequency is nearly constant up to $k_m = 1 \times 10^7$ N/m and thereafter increases sharply, and the third torsional natural frequency increases slowly after $k_m = 1 \times 10^8$ N/m. To examine the change of the second torsional mode shape with increasing values of k_m, the modes at $k_m = 6.31 \times 10^5$ and 6.31×10^9 N/m are shown in Fig. 7. It can be seen that the mode changes from a first torsional mode shape (i.e., crossing the neutral axes once) to a second torsional mode shape (i.e., crossing the neutral axes twice).

3.1.2. *Coupled analysis*

Fig. 8 shows the coupled lateral and torsional natural frequencies versus k_m in which the designations of the torsional natural frequencies are given for convenience, having been determined from the mode shapes at $k_m = 0-1 \times 10^6$ N/m. Compared to the uncoupled analysis results shown in Fig. 6, the lateral vibrations show changes mainly with high order natural frequencies of over 20 000 r.p.m. above $k_m = 1 \times 10^8$ N/m. The characteristics of the torsional

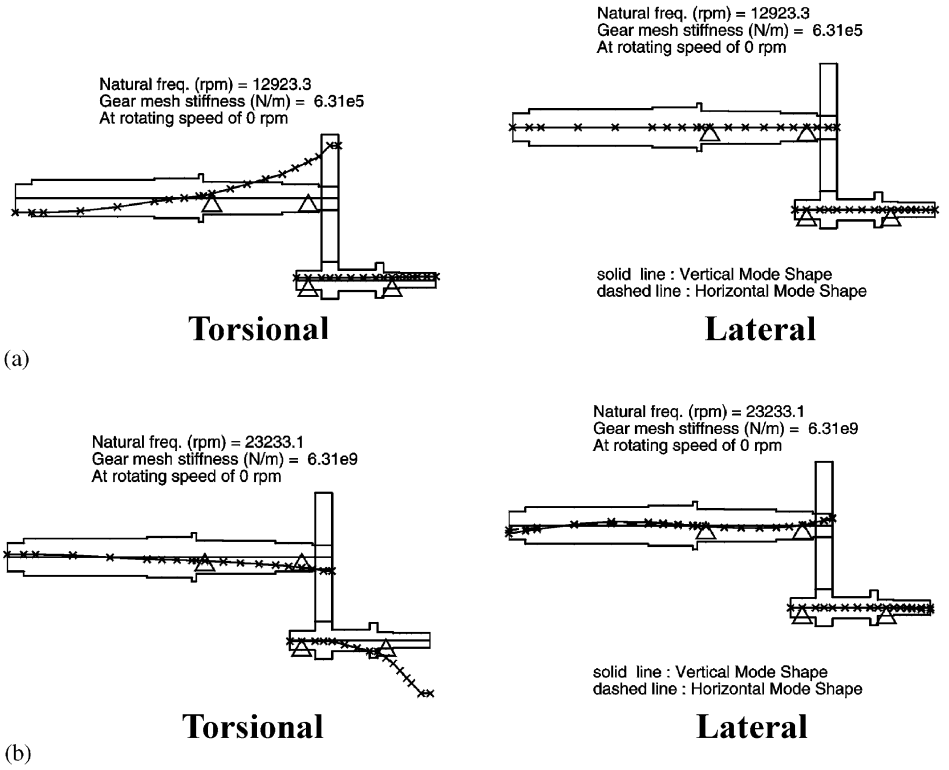

Fig. 9. Second torsional modes and corresponding lateral modes for a coupled analysis at different gear mesh stiffnesses and 0 r.p.m. (a) $k_m = 6.31 \times 10^5$ N/m; (b) $k_m = 6.31 \times 10^9$ N/m.

vibrations indicate that the second torsional natural frequency, in particular, decreases greatly: a 20% reduction in the coupled natural frequency (22 212 r.p.m.) over the uncoupled one (27 763 r.p.m.) at the design gear mesh stiffness is observed. Fig. 9 shows the coupled second torsional modes for the two values of k_m and their associated lateral modes. Even though k_m increases to over 1×10^8 N/m, the torsional mode in Fig. 9(b) does not appear to cross the neutral axis of the compressor shaft, being different from that shown in Fig. 7(b). At this time, the lateral mode of the motor shaft in Fig. 9(b) also shows some change, compared to that in Fig. 9(a) at $k_m = 6.31 \times 10^5$ N/m. As a result, the lateral mode appears to grow due to the coupling effect for values of k_m in excess of 1×10^8 N/m and eventually the torsional mode is retarded, resulting in the torsional mode apparently not crossing the neutral axes twice and the corresponding natural frequency decreasing greatly, compared to the uncoupled one.

3.2. Natural frequency and mode versus gear mesh stiffness at a motor speed of 3420 r.p.m.

3.2.1. Uncoupled analysis

Fig. 10 shows the uncoupled lateral and torsional natural frequencies versus k_m. As k_m increases, the torsional natural frequencies show characteristics identical to those in Fig. 6 at

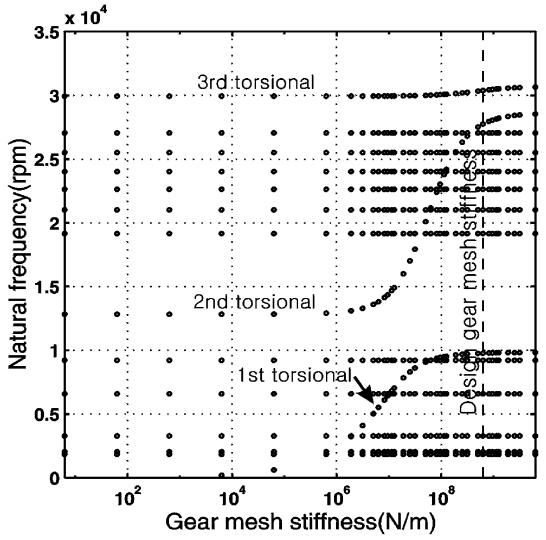

Fig. 10. Natural frequencies versus gear mesh stiffness for an uncoupled analysis at 3420 r.p.m.

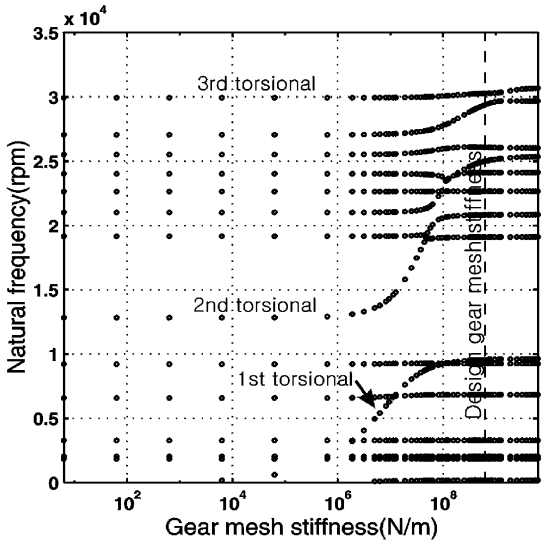

Fig. 11. Natural frequencies versus gear mesh stiffness for a coupled analysis at 3420 r.p.m.

0 r.p.m. However, it can be seen that the gyroscopic effect has an influence on the lateral natural frequencies.

3.2.2. *Coupled analysis*

Fig. 11 shows the coupled lateral and torsional natural frequencies versus k_m in which the designations of the torsional natural frequencies are given, having been determined from

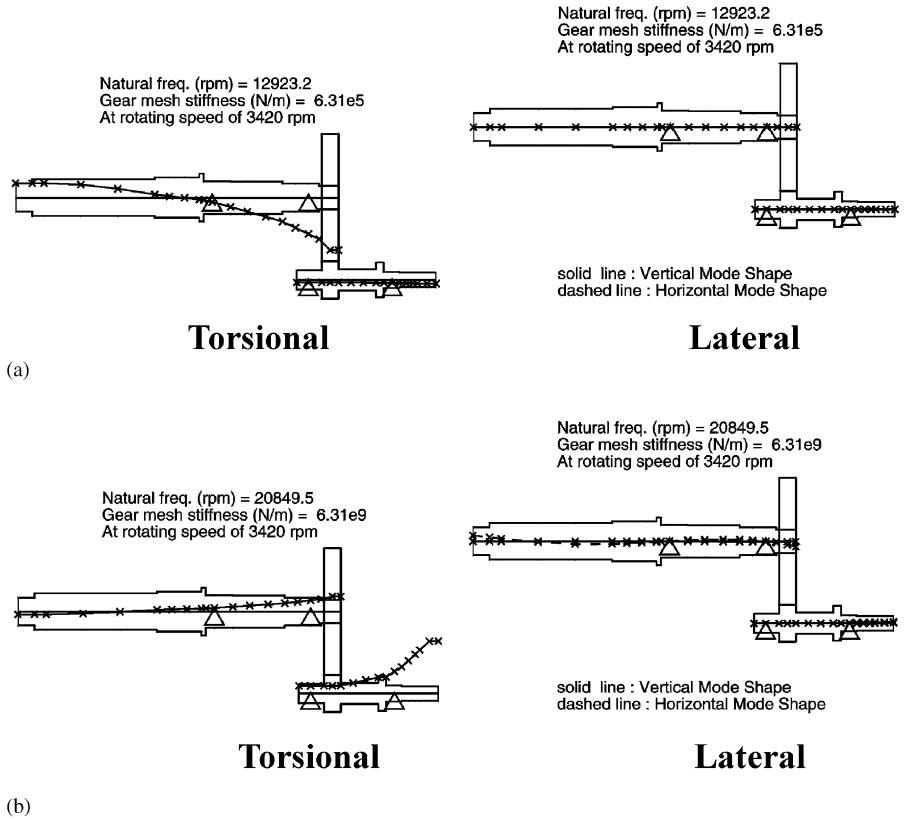

Fig. 12. Second torsional modes and corresponding lateral modes for a coupled analysis at different gear mesh stiffnesses and 3420 r.p.m. (a) $k_m = 6.31 \times 10^5$ N/m; (b) $k_m = 6.31 \times 10^9$ N/m.

the mode shapes at $k_m = 0-1 \times 10^6$ N/m, as before. Compared to the uncoupled analysis results shown in Fig. 10, the lateral vibrations show changes mainly with high order natural frequencies of over 15 000 r.p.m. above $k_m = 1 \times 10^8$ N/m. The characteristics of the torsional vibrations are that, especially, the second torsional natural frequency again decreases greatly: a 25% reduction in the coupled natural frequency (20 832 r.p.m.) over the uncoupled one (27 763 r.p.m.) at the design gear mesh stiffness is observed. Fig. 12 shows the coupled second torsional modes for the two values of k_m and their associated lateral modes. Even though k_m increases to over 1×10^8 N/m, the torsional mode in Fig. 12(b) does not cross the neutral axis of the compressor shaft. Similar to the case at 0 r.p.m., this has resulted because the lateral mode, developed by the coupling effect at a relatively high k_m (over 1×10^8 N/m), has influenced the torsional mode. Further, at a motor speed of 3420 r.p.m. the gyroscopic effect comes into play and eventually the lateral mode becomes greater. Therefore, the torsional mode has been retarded to a greater extent and the coupled second torsional natural frequency has decreased greater over that at 0 r.p.m. (5% more at the design gear mesh stiffness).

3.3. Strain energy of vibration mode

The strain energies of the associated lateral and torsional modes were separately calculated for each natural frequency at the design gear mesh stiffness and a motor speed of 3420 r.p.m. Each dominant mode, determined from the strain energies, was then compared to the initial mode. Here, the initial mode designates the vibration mode type prevailing at $k_m = 0-1 \times 10^6$ N/m where the coupling effect due to gear meshing is negligible.

Table 1 presents the initial modes and the lateral and torsional strain energies for the uncoupled analysis. It can be seen that the initial modes coincide with the dominant modes relative to the strain energies over all the natural frequencies examined in this study. Table 2 shows the initial modes and the lateral and torsional strain energies for the coupled analysis. At the seventh natural frequency of 9573 r.p.m., since the torsional strain energy (0.001) is larger than the lateral strain energy (8.55×10^{-4}), the mode is identified as the coupled first torsional mode, which coincides with the initial mode. In the next case, at the ninth natural frequency of 20 832 r.p.m, since the lateral strain energy (0.05) is larger than the torsional strain energy (0.01), the mode is identified as a lateral one whereas the initial mode represents a torsional one. To investigate this peculiar phenomenon of the coupled second torsional mode at the design gear mesh stiffness, Table 3 presents the second torsional natural frequency versus k_m and the associated lateral and torsional strain energies. The torsional strain energy is larger than the lateral strain energy for values below $k_m = 6.31 \times 10^6$ N/m whereas the lateral strain energy becomes larger for values above $k_m = 6.31 \times 10^7$ N/m. Therefore, it can be concluded that a given dominant mode may change from an initial torsional one to a lateral one as k_m increases. In this case, a coupled torsional mode shape also undergoes some change (see Figs. 7(b) and 12(b)). On the other hand, at the 14th natural frequency of 29 399 r.p.m., as shown in Table 2, the initial mode represents a lateral one whereas the torsional strain energy (0.004) is larger than the lateral strain energy (0.003).

Table 1
Comparisons of lateral and torsional strain energies for an uncoupled analysis at $k_m = 6.31 \times 10^8$ N/m and 3420 r.p.m.

Natural frequency (r.p.m.)	Initial mode	Strain energy		
		Lateral		Torsional
1847	Motor-lateral	24.81	>	1.92e-21
2047	Motor-lateral	0.92	>	3.39e-23
3287	Motor-lateral	0.42	>	8.36e-24
6597	Impeller-lateral	0.12	>	2.43e-22
9223	Impeller-lateral	0.08	>	7.17e-23
9780	Torsional	8.32e-26	<	0.002
19 161	Impeller-lateral	0.003	>	1.16e-24
21 025	Motor-lateral	0.05	>	9.53e-25
22 649	Motor-lateral	0.05	>	9.21e-26
24 032	Motor-lateral	0.06	>	3.66e-24
25 520	Impeller-lateral	0.002	>	7.29e-25
27 067	Motor-lateral	0.05	>	8.90e-25
27 763	Torsional	7.25e-27	<	7.74e-4
30 396	Torsional	0.67e-27	<	2.83e-4

Table 2
Comparisons of lateral and torsional strain energies for a coupled analysis at $k_m = 6.31 \times 10^8$ N/m and 3420 r.p.m.

Natural frequency (r.p.m.)	Initial mode	Strain energy		
		Lateral		Torsional
191	Motor-lateral	0.22	>	0.03
1849	Motor-lateral	0.52	>	0.08
2047	Motor-lateral	0.72	>	0.08
3288	Motor-lateral	0.40	>	0.16
6839	Impeller-lateral	0.08	>	0.04
9254	Impeller-lateral	0.06	>	3.26e-4
9573	Torsional	8.55e-4	<	0.001
19 099	Impeller-lateral	0.006	>	3.27e-4
20 832	Torsional	0.05	>	0.01
22 668	Motor-lateral	0.08	>	0.001
24 119	Motor-lateral	0.04	>	0.002
25 015	Motor-lateral	0.0113	>	0.0108
26 091	Impeller-lateral	0.003	>	5.12e-4
29 399	Motor-lateral	0.003	<	0.004
30 281	Torsional	0.001	<	0.01

Table 3
Comparisons of lateral and torsional strain energies associated with the coupled 2nd torsional mode as a function of k_m at 3420 r.p.m.

k_m (N/m)	Natural frequency (r.p.m.)	Strain energy		
		Lateral		Torsional
6.31e3	12 836	2.92e-10	<	0.07
6.31e5	12 923	2.36e-6	<	0.07
6.31e6	13 792	6.69e-5	<	0.01
6.31e7	20 075	0.004	>	0.002
6.31e8	20 832	0.05	>	0.01
6.31e9	20 850	0.12	>	0.08

Table 4
Comparisons of lateral and torsional strain energies associated with the coupled 14th lateral mode as a function of k_m at 3420 r.p.m.

k_m (N/m)	Natural frequency (r.p.m.)	Strain energy		
		Lateral		Torsional
6.31e3	27 067	0.03	>	1.96e-11
6.31e5	27 071	0.05	>	8.18e-8
6.31e6	27 108	0.04	>	2.15e-5
6.31e7	27 500	0.02	>	1.64e-4
6.31e8	29 399	0.003	<	0.004
6.31e9	29 690	0.001	<	0.003

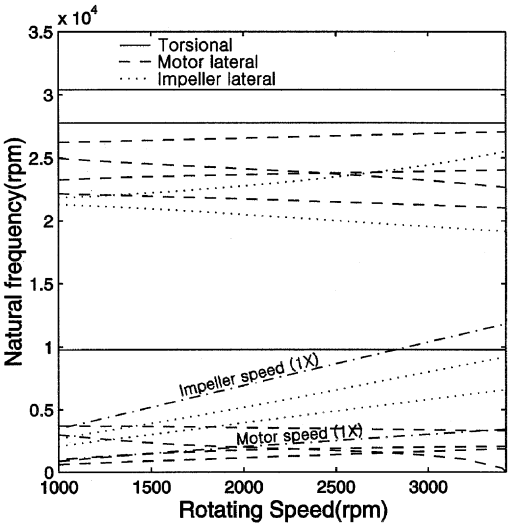

Fig. 13. Campbell diagram for an uncoupled analysis at $k_m = 6.31 \times 10^8$ N/m.

Similarly, Table 4 presents the 14th coupled natural frequency versus k_m and the associated lateral and torsional strain energies. The lateral strain energy is larger than the torsional strain energy for values below $k_m = 6.31 \times 10^7$ N/m whereas the torsional strain energy becomes larger for values above $k_m = 6.31 \times 10^8$ N/m. Therefore, it can also be concluded that a given dominant mode may change from an initial lateral one to a torsional one as k_m increases.

3.4. Campbell diagram analysis

Fig. 13 shows a Campbell diagram for the uncoupled analysis at the design gear mesh stiffness. As expected, the torsional natural frequencies remain constant regardless of the rotating speed. Fig. 14 shows a Campbell diagram for the coupled analysis in which a distinction between the lateral and torsional vibrations has been made from a mode type at $k_m = 0{-}1 \times 10^6$ N/m, as before. A comparison of Figs. 13 and 14 shows that for low order lateral whirl natural frequencies below 15 000 r.p.m. there are no practical effects associated with a speed change whereas for high order lateral whirl natural frequencies above 15 000 r.p.m. some effects associated with a speed change are evident. In addition, the coupled first, second and third torsional natural frequencies decrease by 1.28%, 5.05% and 0.71%, respectively, again due to the growth of the coupled lateral modes as the motor speed increases from 1000 to 3420 r.p.m.

4. Conclusions

By applying a coupled lateral and torsional vibration finite element model of a gear pair, this paper provides a detailed examination of the coupled vibration characteristics of a turbo-chiller rotor-bearing system containing a bull-pinion speed increasing gear. The results show that some

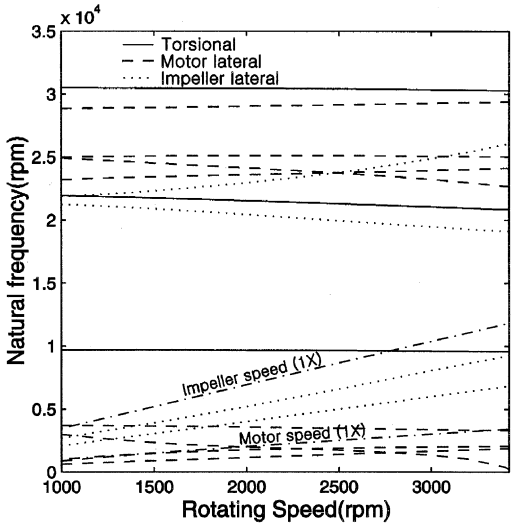

Fig. 14. Campbell diagram for a coupled analysis at $k_m = 6.31 \times 10^8$ N/m.

modes may yield coupled lateral and torsional mode characteristics as the gear mesh stiffness increases over a certain value and, moreover, that their associated dominant modes may be different from their initial modes, i.e., a given dominant mode may change from an initial torsional one to a lateral one or vice versa. In particular, for the case of the second torsional natural frequency, the torsional strain energy decreases due to a retardation of the torsional mode in conjunction with a growth in the lateral mode at the design gear mesh stiffness and eventually the coupled torsional natural frequency decreases by 25% over the uncoupled one at the rated speed.

Appendix A

$$[M^{G'}] = \begin{bmatrix} M_1^G & 0 & 0 & 0 & 0 & 0 & 0 & 0 & 0 & 0 \\ 0 & M_1^G & 0 & 0 & 0 & 0 & 0 & 0 & 0 & 0 \\ 0 & 0 & I_{t1}^G & 0 & 0 & 0 & 0 & 0 & 0 & 0 \\ 0 & 0 & 0 & I_{t1}^G & 0 & 0 & 0 & 0 & 0 & 0 \\ 0 & 0 & 0 & 0 & M_2^G & 0 & 0 & 0 & 0 & 0 \\ 0 & 0 & 0 & 0 & 0 & M_2^G & 0 & 0 & 0 & 0 \\ 0 & 0 & 0 & 0 & 0 & 0 & I_{t2}^G & 0 & 0 & 0 \\ 0 & 0 & 0 & 0 & 0 & 0 & 0 & I_{t2}^G & 0 & 0 \\ 0 & 0 & 0 & 0 & 0 & 0 & 0 & 0 & I_{p1}^G & 0 \\ 0 & 0 & 0 & 0 & 0 & 0 & 0 & 0 & 0 & I_{p2}^G \end{bmatrix}, \tag{A.1}$$

$$[C^{G'}] = c_m \begin{bmatrix} 0 & 0 & 0 & 0 & 0 & 0 & 0 & 0 & 0 & 0 \\ 0 & 1 & 0 & 0 & 0 & -1 & 0 & 0 & r_1 & r_2 \\ 0 & 0 & 0 & 0 & 0 & 0 & 0 & 0 & 0 & 0 \\ 0 & 0 & 0 & 0 & 0 & 0 & 0 & 0 & 0 & 0 \\ 0 & 0 & 0 & 0 & 0 & 0 & 0 & 0 & 0 & 0 \\ 0 & -1 & 0 & 0 & 0 & 1 & 0 & 0 & -r_1 & -r_2 \\ 0 & 0 & 0 & 0 & 0 & 0 & 0 & 0 & 0 & 0 \\ 0 & 0 & 0 & 0 & 0 & 0 & 0 & 0 & 0 & 0 \\ 0 & r_1 & 0 & 0 & 0 & -r_1 & 0 & 0 & r_1^2 & r_1 r_2 \\ 0 & r_2 & 0 & 0 & 0 & -r_2 & 0 & 0 & r_1 r_2 & r_2^2 \end{bmatrix}, \tag{A.2}$$

$$[G^{G'}] = \begin{bmatrix} 0 & 0 & 0 & 0 & 0 & 0 & 0 & 0 & 0 & 0 \\ 0 & 0 & 0 & 0 & 0 & 0 & 0 & 0 & 0 & 0 \\ 0 & 0 & 0 & I_{p1}^G \Omega_1 & 0 & 0 & 0 & 0 & 0 & 0 \\ 0 & 0 & -I_{p1}^G \Omega_1 & 0 & 0 & 0 & 0 & 0 & 0 & 0 \\ 0 & 0 & 0 & 0 & 0 & 0 & 0 & 0 & 0 & 0 \\ 0 & 0 & 0 & 0 & 0 & 0 & 0 & 0 & 0 & 0 \\ 0 & 0 & 0 & 0 & 0 & 0 & 0 & I_{p2}^G \Omega_2 & 0 & 0 \\ 0 & 0 & 0 & 0 & 0 & 0 & -I_{p2}^G \Omega_2 & 0 & 0 & 0 \\ 0 & 0 & 0 & 0 & 0 & 0 & 0 & 0 & 0 & 0 \\ 0 & 0 & 0 & 0 & 0 & 0 & 0 & 0 & 0 & 0 \end{bmatrix}, \tag{A.3}$$

$$[K^{G'}] = k_m \begin{bmatrix} 0 & 0 & 0 & 0 & 0 & 0 & 0 & 0 & 0 & 0 \\ 0 & 1 & 0 & 0 & 0 & -1 & 0 & 0 & r_1 & r_2 \\ 0 & 0 & 0 & 0 & 0 & 0 & 0 & 0 & 0 & 0 \\ 0 & 0 & 0 & 0 & 0 & 0 & 0 & 0 & 0 & 0 \\ 0 & 0 & 0 & 0 & 0 & 0 & 0 & 0 & 0 & 0 \\ 0 & -1 & 0 & 0 & 0 & 1 & 0 & 0 & -r_1 & -r_2 \\ 0 & 0 & 0 & 0 & 0 & 0 & 0 & 0 & 0 & 0 \\ 0 & 0 & 0 & 0 & 0 & 0 & 0 & 0 & 0 & 0 \\ 0 & r_1 & 0 & 0 & 0 & -r_1 & 0 & 0 & r_1^2 & r_1 r_2 \\ 0 & r_2 & 0 & 0 & 0 & -r_2 & 0 & 0 & r_1 r_2 & r_2^2 \end{bmatrix}, \tag{A.4}$$

$$\{Q^{G'}\} = \begin{bmatrix} U_1\Omega_1^2 \cos \Omega_1 t \\ U_1\Omega_1^2 \sin \Omega_1 t + F_1 \\ 0 \\ 0 \\ U_2\Omega_2^2 \cos \Omega_2 t \\ U_2\Omega_2^2 \sin \Omega_2 t - F_1 \\ 0 \\ 0 \\ F_s e_1 \cos \Omega_1 t - F_1 r_1 \\ F_s e_2 \cos \Omega_2 t - F_1 r_2 \end{bmatrix}, \tag{A.5}$$

where

$$\begin{aligned} F_1 = {} & k_m[e_2 \sin \Omega_2 t - e_1 \sin \Omega_1 t + e_t \sin(N_1\Omega_1 t)] \\ & + c_m[e_2\Omega_2 \cos \Omega_2 t - e_1\Omega_1 \cos \Omega_1 t + e_t N_1\Omega_1 \cos(N_1\Omega_1 t)] \end{aligned} \tag{A.6}$$

and

$$F_s = k_m[-v_1^{G'} - r_1\Omega_1 t + v_2^{G'} - r_2\Omega_2 t] + c_m[-\dot{v}_1^{G'} - r_1\Omega_1 + \dot{v}_2^{G'} - r_2\Omega_2] - F_1, \tag{A.7}$$

$$[T] = c_m \begin{bmatrix} -S & C & 0 & 0 & 0 & 0 & 0 & 0 & 0 & 0 \\ -C & -S & 0 & 0 & 0 & 0 & 0 & 0 & 0 & 0 \\ 0 & 0 & -S & C & 0 & 0 & 0 & 0 & 0 & 0 \\ 0 & 0 & -C & -S & 0 & 0 & 0 & 0 & 0 & 0 \\ 0 & 0 & 0 & 0 & -S & C & 0 & 0 & 0 & 0 \\ 0 & 0 & 0 & 0 & -C & -S & 0 & 0 & 0 & 0 \\ 0 & 0 & 0 & 0 & 0 & 0 & -S & C & 0 & 0 \\ 0 & 0 & 0 & 0 & 0 & 0 & -C & -S & 0 & 0 \\ 0 & 0 & 0 & 0 & 0 & 0 & 0 & 0 & 1 & 0 \\ 0 & 0 & 0 & 0 & 0 & 0 & 0 & 0 & 0 & 1 \end{bmatrix}. \tag{A.8}$$

References

[1] R.L. Eshleman, R.A. Eubanks, On the critical speeds of a continuous rotor, American Society of Mechanical Engineers Journal of Engineering for Industry (1969) 1180–1188.

[2] L.D. Mitchell, D.M. Mellen, Torsional-lateral coupling in a geared high-speed rotor system, ASME Paper 75-DET-75, 1975.

[3] J.W. Lund, Critical seeds stability and response of a geared train of rotors, American Society of Mechanical Engineers Journal of Mechanical Design 100 (1978) 535–539.

[4] H. Iida, A. Tamura, K. Kikuch, H. Agata, Coupled torsional–flexural vibration of a shaft in a geared system of rotors (1st report), Bulletin of the JSME 23 (186) (1980) 2111–2117.
[5] T. Iwatsubo, S. Arii, R. Kawai, Coupled lateral-torsional vibration of rotor system trained by gears, Bulletin of the JSME 27 (224) (1984) 271–277.
[6] S.V. Neriya, R.B. Bhat, T.S. Sanker, Effect of coupled torsional-flexural vibration of a geared shaft system on dynamic tooth load, The Shock and Vibration Bulletin Part 3 54 (1984) 67–75.
[7] A. Kahraman, H.N. Ozguven, D.R. Houser, J.J. Zakrajsek, Dynamic analysis of geared rotors by finite elements, American Society of Mechanical Engineers Journal of Mechanical Design 114 (1992) 507–514.
[8] J.S. Rao, J.R. Chang, T.N. Shiau, Coupled bending-torsion vibration of geared rotors, ASME DE-Vol. 84-2, Design Engineering Technical Conferences, Vol. 3, Part B, 1995, pp. 977–989.
[9] A.S. Lee, J.W. Ha, D.-H. Choi, A coupled lateral and torsional FE rotordynamic analysis of speed increasing geared rotor-bearing system, Journal of KSNVE 11 (1) (2001) 82–88 (in Korean).
[10] S.T. Choi, S.Y. Mau, Dynamic analysis of geared rotor-bearing systems by the transfer matrix method, ASME DE-Vol. 84-2, Design Engineering Technical Conferences, Vol. 3, Part B, 1995, pp. 967–976.
[11] A.S. Lee, Y.-S. Lee, Rotordynamic characteristics of an APU gas turbine rotor-bearing system having a tie shaft, KSME International Journal 15 (2) (2001) 152–159.
[12] J.-J. Jeon, A study on the vibration of the spur gear system, Master Thesis, KAIST, Korea, 1984 (in Korean).